Astron. Astrophys. 330, 1149–1159 (1998)

ASTRONOMY AND ASTROPHYSICS

Inferring the equatorial solar tachocline from frequency splittings

T. Corbard, G. Berthomieu, J. Provost, and P. Morel

Laboratoire G.-D. Cassini, CNRS UMR 6529, Observatoire de la Côte d'Azur, BP 4229, F-06304 Nice Cedex 4, France

Received 17 July 1997 / Accepted 24 October 1997

Abstract. Helioseismic inversions, carried out for several years on various ground-based and spatial observations, have shown that the solar rotation rate presents two principal regimes: a quasi-rigid rotation in the radiative interior and a latitude-dependent rotation in the whole convection zone. The thin layer, named solar tachocline, between these two regimes is difficult to infer through inverse techniques because of the ill-posed nature of the problem that requires regularization techniques which, in their global form, tend to smooth out any high gradient in the solution. Thus, most of the previous attempts to study the rotation profile of the solar tachocline have been carried out through forward modeling. In this work we show that some appropriate inverse techniques can also be used and we compare the ability of three 1D inverse techniques combined with two automatic strategies for the choice of the regularization parameter, to infer the solar tachocline profile in the equatorial plane. Our work, applied on LOWL (LOWL is an abbreviation for low degree denoted by L) two years dataset, argue in favor of a very sharp ($0.05 \pm 0.03 R_\odot$) transition zone located at $0.695 \pm 0.005 R_\odot$ which is in good agreement with the previous forward analysis carried out on Global Oscillations Network Group (GONG), Big Bear Solar Observatory (BBSO) and LOWL datasets.

Key words: Sun: interior – Sun: oscillations – Sun: rotation – methods: numerical

1. Introduction

Helioseismic inversions of the solar p-modes frequencies splitted by rotation have shown that there is, at the base of the convection zone, a thin transition layer separating two regimes of rotation, a strong differential rotation in the convection zone and a quasi rigid rotation in the radiative interior (e.g. Thompson et al. 1996; Corbard et al. 1997). This layer, called tachocline, is supposed to play an important role in the solar dynamo, in the transport of angular momentum and in the mixing of chemical elements. Its position r_c and thickness w give constraints to the theories describing its structure and evolution (Spiegel & Zahn 1992; Gough & Sekii 1997). Different estimations of these parameters have been obtained so far mostly by using forward methods (Kosovichev 1996; Charbonneau et al. 1997; Basu 1997).

The aim of this work is to test and compare the ability of some inversion methods to infer the location and the width of the solar tachocline, and then to apply these methods to helioseismic data. We compare three 1D least-squares methods. They differ essentially by the mean used to regularize the ill-posed inverse problem of inferring the equatorial solar rotation rate from the observed frequency splittings. The first method is the most commonly used Regularized Least-Squares (RLS) method with Tikhonov regularization (Tikhonov & Arsenin 1977), the second one is the Modified Truncated Singular Value Decomposition (MTSVD) introduced by Sekii and Shibahashi (1988) which uses a regularization term of the same form but with a discrete truncation parameter instead of the continuous Tikhonov regularization parameter. The third method, introduced by Hansen & Mosegaard (1996), is called Piecewise Polynomials TSVD (PP-TSVD) and is a modification of the MTSVD method that can preserve discontinuities of the solution.

In Sect. 2, we briefly recall the inverse problem and define our parameterization of the tachocline. Sect. 3 gives the two strategies studied in this work for inferring the rapid variation of the rotation. We test these methods by inverting artificial data in Sect. 4 and then, in Sect. 5, we use this study in order to infer the location and thickness of the solar tachocline in the equatorial plane from data observed by the LOWL instrument (Tomczyk et al. 1995).

2. Direct analysis and parameterization of the tachocline

Frequency splittings $\Delta\nu_{nlm} = \nu_{nlm} - \nu_{nl-m}$ between modes with the same radial order n and degree l but different azimuthal orders m are induced by the solar rotation $\Omega(r,\theta)$ expressed as a function of the radius r and colatitude θ. For a slow rotation, assumed to be symmetric about the equator, and moderate or high degree modes, these splittings are given by:

$$\Delta\nu_{nlm} = m \int_0^{\frac{\pi}{2}} \int_0^{R_\odot} K_{nl}(r) P_l^m(\cos\theta)^2 \; \Omega(r,\theta) \; \sin\theta \; dr \; d\theta, \quad (1)$$

Send offprint requests to: T. Corbard

where $K_{nl}(r)$ are the so-called rotational kernels that can be calculated for each mode from a solar model (Morel et al. 1997). In the following, they are assumed to be known exactly. There exists additional terms that are not taken into account in Eq. (1) but, as discussed in Corbard et al. (1997), they do not influence inversion above $0.4R_\odot$. As the aim of this work is not to sound the rotation of the core, Eq. (1) is a good approximation. $P_l^m(\cos\theta)$ are normalized Legendre functions. Their asymptotic property leads, as discussed by Antia et al. (1996), to the following expression that shows the sectoral (i.e. $l = m$) modes splittings as weighted averages of the equatorial rotation rate $\Omega_{eq}(r) = \Omega(r, 90°)$:

$$\Delta\nu_{nll} \simeq l \int_0^{R_\odot} K_{nl}(r)\, \Omega_{eq}(r)\, dr. \tag{2}$$

We note that the validity of this 1D approximation is l-dependent. Indeed, the higher the degree, the more the latitudinal kernel $P_l^l(\cos\theta)^2 \sin\theta$ is peaked at the equator.

Following Charbonneau et al. (1997), we define the location and the width of the transition zone in the equatorial plane as the parameters $\hat{r}_c$ and $\hat{w}$ respectively of the following erf function which fits the rotation law in this plane:

$$\Omega_{eq}(r) = \hat{\Omega}_0 + \frac{1}{2}(\hat{\Omega}_1 - \hat{\Omega}_0)\left(1 + erf\left(\frac{r - \hat{r}_c}{0.5\hat{w}}\right)\right). \tag{3}$$

Here $\hat{\Omega}_0$ and $\hat{\Omega}_1$ represent the mean values of the rotation in the radiative interior and in the convection zone respectively.

In order to compare different 1D inverse methods, we have built several sets of theoretical sectoral frequency splittings that correspond to different given rotation laws with fixed parameters r_c, w, Ω_0, Ω_1 but with a function of the colatitude in order to mimic the latitudinal differential rotation of the convection zone:

$$\Omega(r,\theta) = \Omega_0 + \frac{1}{2}(\Omega_1 - A\cos^2\theta - B\cos^4\theta - \Omega_0)\left(1 + erf\left(\frac{r - r_c}{0.5w}\right)\right) \tag{4}$$

Evidently, for any choice of constants A and B, the searched parameters for these rotation laws are $\hat{r}_c = r_c$, $\hat{w} = w$, $\hat{\Omega}_0 = \Omega_0$ and $\hat{\Omega}_1 = \Omega_1$. We compute the splittings $\Delta\nu_{nll}$ from Eq. (1) for a set of modes corresponding to the set of LOWL data used in Corbard et al. (1997) and we add a normally distributed noise $\delta\nu_{nll} \in \mathcal{N}(0, \sigma_{nl})$. For each mode (n, l) the standard deviation of the noise σ_{nl} has been taken equal to:

$$\sigma_{nl} = \frac{\bar{\sigma}_{nl}}{\sqrt{k_\sigma}}, \tag{5}$$

where $\bar{\sigma}_{nl}$ is the error derived from the observers' uncertainties for a splitting $\Delta\nu_{nll}$, and k_σ is an integer used to vary the level of the noise that we introduce in the data. Doing this, we take into account the fact that the error obtained on the observed splitting varies with the frequency and the degree of the mode which is certainly more realistic than taking the same average standard deviation for all the modes. From those noisy splittings, the equatorial rotation profile is obtained by inverting Eq. (2) and this profile is then fitted by the erf function Eq. (3) leading to the parameters $\bar{r}_c$, $\bar{w}$, $\bar{\Omega}_0$, $\bar{\Omega}_1$ which will be compared to the initial parameters.

3. Strategies for inferring rapid variations of the rotation

The three inverse methods used in this work are detailed in Appendix A. They all use a grid of 50 points in radius distributed according to the density of turning points of observed modes. The most important difficulty in inferring the thickness of the tachocline from inverse methods results from the fact that the problem of solving Eq. (2) is an ill-posed problem and this is strengthened by the fact that rotational kernels give redundant information about the outer part of the sun whereas they have only low amplitude in the solar core for the observed mode set. Numerically, this produces a high value for the condition number (defined as the maximum singular value divided by the smallest singular value) of the discretized problem Eq. (A5) (typically $\Lambda_{max}/\Lambda_{min} \simeq 2 \times 10^8$ in our implementation) and the singular values decay rapidly. This high value of the condition number means that the solution of the initial problem is highly sensitive to the numerical errors and the noise contained in the data. Therefore we have to introduce some a-priori knowledge on the rotation profile. Unfortunately this regularization tends to smooth out every rapid variation in the solution. By using global regularization, we make the implicit assumption that the real rotation is smooth everywhere and therefore the information about the thickness of a rapid variation of the rotation profile is not directly readable from the solutions obtained by classic inversions. There are however several ways for overcoming these difficulties.

3.1. Local deconvolution of the result obtained from linear inversions: the use of averaging kernels

The first way is to have a good understanding of the process by which the inversion smoothes the solution: using this information, we may be able to inverse this process and to acquire a more realistic view of the rotation. This is what Charbonneau et al. (1997) have done in combination with the so-called Subtractive Optimal Localized Average (SOLA) (Pijpers & Thompson 1992, 1994) method. This can be generalized for any linear inversion as RLS method used in this work. The solution $\bar{\Omega}(r_0)$ obtained at a target location r_0 can be viewed as a weighted average of the 'true rotation' $\Omega(r)$, the weighting function being the averaging kernel $\kappa(r, r_0)$ that can always be estimated at any r_0:

$$\bar{\Omega}(r_0) = \int_0^{R_\odot} \kappa(r, r_0)\Omega(r)\, dr. \tag{6}$$

If we suppose that the averaging kernels obtained at any depth can be approximated by a translation of the averaging kernel obtained at the middle of the transition i.e. $\kappa(r, \hat{r}_c)$, then we can define κ_c by $\kappa_c(r - \hat{r}_c) \equiv \kappa(r, \hat{r}_c)$ and Eq. (6) reduces to a convolution equation:

$$\bar{\Omega}(r_0) = \int_0^{R_\odot} \kappa_c(r - r_0)\Omega(r)\, dr \Leftrightarrow \bar{\Omega}(r) = \kappa_c(r) * \Omega(r) \tag{7}$$

Finally, if the 'true rotation' can be well approximated by an erf function of the form given by Eq. (3), and if we approximate the kernel $\kappa_c(r-r_0)$ by a Gaussian function of the form:

$$\kappa_c(r-r_0) \simeq \exp\left[-(r-r_0)^2/\Delta_r^2\right], \tag{8}$$

then the inferred solution is also an erf function of the form Eq. (3) but with a larger width $\bar{w}$. A simple deconvolution gives the following relation between the searched width $\hat{w}$ and the inferred width $\bar{w}$:

$$\hat{w} = \bar{w}_c \equiv \sqrt{\bar{w}^2 - 4\Delta_r^2}, \tag{9}$$

which defined the corrected inferred width $\bar{w}_c$.

This result is valid only under a large number of assumptions that may be quite distant from the reality. Especially the reduction to a convolution form is certainly not valid because of the extent of averaging kernels that tend to increase rapidly toward the solar core. Moreover the profile of the rotation rate may be much more complicated than a simple erf function. However, the tachocline is thin and the averaging kernels have nearly the same profile in its whole extent. Thus this is certainly a good approach to get a quantitative idea of how the inversion enlarges the 'true rotation' transition. We note that if we obtain $\Delta_r > \bar{w}/2$ this certainly means that some of the previous assumptions are not valid. In this work, we have applied this 'deconvolution method' on the solutions obtained by Tikhonov inversions computed as explained in Appendix A.1.. We estimate that this cannot be made for MTSVD method because the corresponding averaging kernels are less well peaked and exhibit a more oscillatory behavior (see Fig. 6 hereafter).

3.2. Non linear regularization

The second way to estimate the location and thickness of the tachocline, is to build inverse methods that are capable of producing solutions with steep gradients. The idea is to apply a local regularization instead of the global Tikhonov regularization term. This leads to a non linear problem and piecewise smooth solutions. This approach has recently found useful applications in image processing for edge-preserving regularization (Aubert et al. 1994) and total variation (TV) denoising (Vogel & Oman 1996, 1997). In particular, the TV of f is defined as the 1-norm of the first derivative of f and this is the definition of smoothness that we use in the PP-TSVD inverse method. Therefore, the results obtained by this method, detailed in Appendix A.2., represent a first attempt to use this class of inversion with non linear regularization on helioseismic data.

4. Tests with artificial data: results and discussion

4.1. The key: how to choose regularization parameters

Whichever regularized inverse method we use, a very important point is the choice of the regularization parameter which can be a discrete truncation parameter k (MTSVD, PP-TSVD, Eq. (A12)) or a continuous parameter λ (Tikhonov, Eq. (A9)). This choice is specially important if we want to infer a quantity like the width of a zone with high gradients which is directly affected by the regularization. Several methods for choosing the regularization parameter have been proposed that tend to establish a balance between the propagation of input errors and the regularization (see e.g. Badeva & Morozov (1991), Thompson & Craig (1992) and Hansen (1992, 1994) for a general review and Thompson (1992), Barett (1993) and Stepanov & Christensen-Dalsgaard (1996) for applications in helioseismic inversions). In this work we test and compare the ability of two of these automatic strategies, namely the L-curve criterion (Hansen 1992) and the Generalized Cross Validation (GCV) criterion (Wahba 1977; Golub et al. 1979), to reproduce a good estimation of the tachocline profile from noisy data.

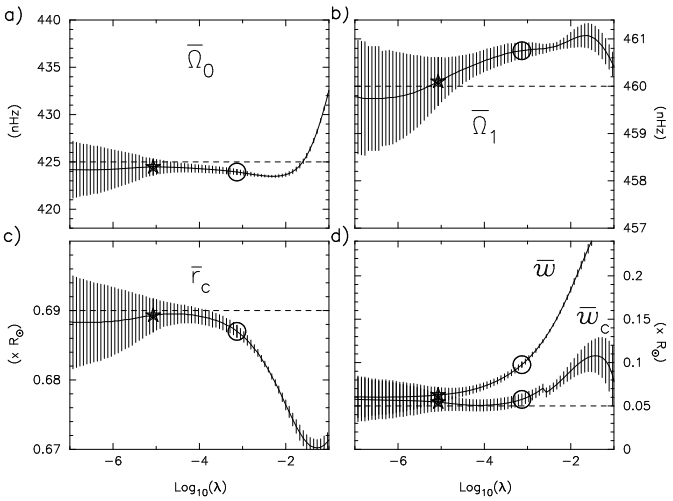

Fig. 1a–d. Inferred parameters $\bar{\Omega}_0$, $\bar{\Omega}_1$, $\bar{r}_c$, $\bar{w}$ and corrected inferred parameter $\bar{w}_c$ against the logarithm of the Tikhonov regularization parameter λ. Error bars result from the fit of the solution by an erf function taking into account the propagation of noise through the inverse process but not the existing correlations between the results obtained at two different radius. The initial parameters are indicated by dashed lines. The GCV and L-curve choices are shown by the full star and the circle respectively. The input rotation law was not dependent on the latitude ($A = B = 0$) and the level of noise was small ($k_\sigma = 10$).

The importance of the choice of the regularization parameter can be illustrated by the following figures (Figs. 1, 2, 3, 4) where the results of the fit of the solution by an erf function are plotted as a function of the regularization parameter.

Fig. 1 represents the variation of the four erf-parameters $\bar{\Omega}_0$, $\bar{\Omega}_1$, $\bar{r}_c$ and $\bar{\omega}$ deduced from a Tikhonov inversion as a function of the logarithm of the regularization parameter. The four initial parameters were $\Omega_0 = 425$ nHz, $\Omega_1 = 460$ nHz, $r_c = 0.69R_\odot$ and $w = 0.05R_\odot$. In this case, called the 'ideal case' in the following, the added errors were small (k_σ=10) and the initial rotation law was not dependent on the latitude ($A = B = 0$). The choices designated by L-curve and GCV strategies are shown by the full star and the circle respectively. In addition we have plotted the corrected inferred width $\bar{w}_c$ given by Eq. (9) and computed by calculating systematically the averaging kernel at $r_0 = \bar{r}_c$ (as shown on Fig. 6a for the

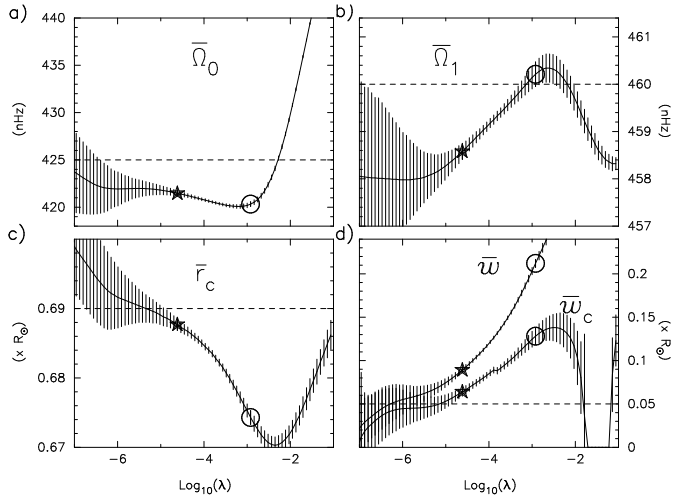

Fig. 2a–d. The same as in Fig. 1 but with more realistic input errors (k_σ = 1) and an input rotation profile with latitudinal variation in the convection zone (A = 55 nHz, B = 75 nHz).

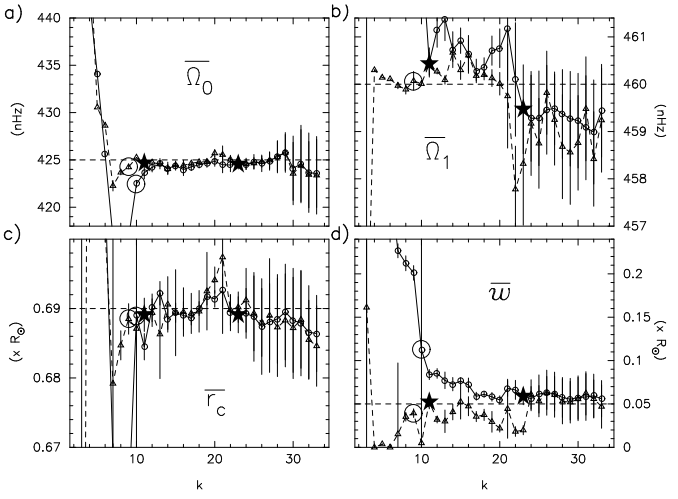

Fig. 3a–d. The same as in Fig. 1 ('ideal case') but for MTSVD (full line) and PP-TSVD (dashed line) methods and against the truncation parameter k. The L-curve choice for MTSVD method is outside the plot on panel **b**.

GCV choice). The GCV criterion leads always to a lower regularization than the L-curve choice and then tends to reduce the smoothing of the solution. In most of our tests, as in Figs. 1a, c, d, the GCV choice corresponds to a point where the errors deduced from the fit become small whereas the L-curve criterion gives a point beyond which a rapid variation of the fitted parameters with increasing regularization occurs. The fact that the values of the fitted parameters are nearly constant between these two points shows that, for this level of noise, the method is robust in that sense that the choice of the precise value of the regularization parameter is not a crucial point: any choice that tends to establish a balance between the propagation of input errors and the regularization is able to produce good results.

Let us now look at the behavior of this method for a more realistic example. For this we take a level of noise similar to the one given by observers (k_σ = 1) and we build frequency splittings of sectoral modes by taking into account a latitudinal variation of the rotation rate in the convection zone close to that derived by 2D inversions. We have set A = 55 nHz and B = 75 nHz which are mean values derived from observations of the plasma motion at the solar surface (Snodgrass & Ulrich 1990). This choice for the input rotation law and errors is referred as the 'realistic case' in the following. The Eq. (1) with $m = l$ has been used to compute the frequency splittings of sectoral modes and 1D Tikhonov inversions have been performed again in order to infer the equatorial rotation rate from Eq. (2).

Fig. 2 represents the results of these inversions in the same form as Fig. 1 and for the same initial erf-parameters. There are two essential points to be seen on this figure. The parameter Ω_0 in Fig. 2a is systematically under-estimated of about 4 nHz. A detailed analysis shows that this effect is strongly related to the introduction of a latitudinal variation of the rotation rate in the convection zone. The assumption, used in the 1D inversions, that sectoral modes are sensitive only to the equatorial component of the rotation rate is not valid for low degree l modes (e.g. Antia et al. 1996) , and these modes sound the deep interior. This may explain some perturbation for the determination of the parameter Ω_0 that represents the mean value of the rotation rate in the radiative interior. The difference between splittings of sectoral modes computed from Eq. (2) and Eq. (1) is below 1 nHz for the observed modes having their turning points above $0.4R_\odot$. The large resulting difference in Ω_0 is due to the fact that high l sectoral modes see only the equatorial rotation rate and then fix the inferred value $\bar{\Omega}_1$ equal (or nearly equal as in Fig. 2b) to the initial value Ω_1 while lower degrees sectoral modes are sensitive to the differential rotation of the convection zone and this effect can only be accounted for in the inverse rotation law by a substantial lowering in $\bar{\Omega}_0$. Furthermore we have checked that two rotation laws with the same Ω_1 but with a difference of 4 nHz in Ω_0 and two rotation laws with the same Ω_0 but with or without latitudinal variation in the convection zone, induce a difference of the same order in the sectoral modes frequency splittings.

The second important point is that, in Figs. 2c, d, the estimation $\bar{w}$ of the width of the tachocline increases rapidly between the GCV and the L-curve points whereas its location $\bar{r}_c$ decreases rapidly from $0.688R_\odot$ down to $0.674R_\odot$ As in Fig. 1d, the deconvolution made by using averaging kernels tends to correct this behavior for the estimation of the width but, in this case, the GCV choice remains over-estimated for about $0.015R_\odot$ and the L-curve choice is still very distant from the initial value. Tests made with different input parameters show that, as in Figs. 2c, d and for that level of noise, the GCV choice is always better than the L-curve choice for the estimation of the location and the width of the tachocline. This point will be illustrated and discussed in the next section for the estimation of widths between 0.03 and $0.11R_\odot$.

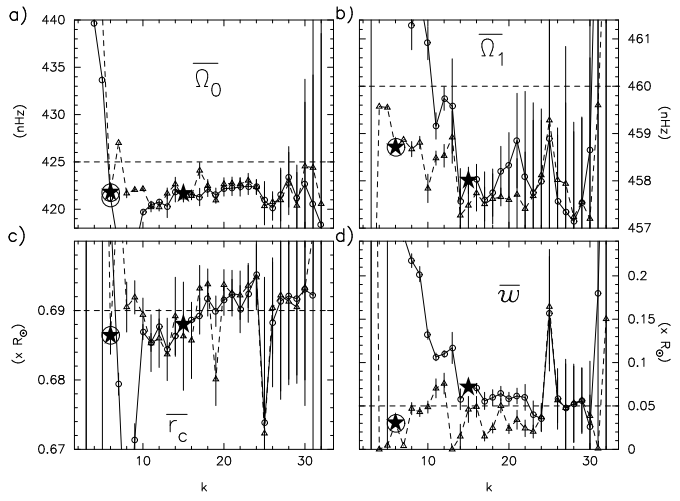

Fig. 4a–d. The same as in Fig. 2 ('realistic case') but for MTSVD (full line) and PP-TSVD (dashed line) methods and against the truncation parameter k. The L-curve choice for MTSVD method is outside the plot on panels **b**,**c** and **d**.

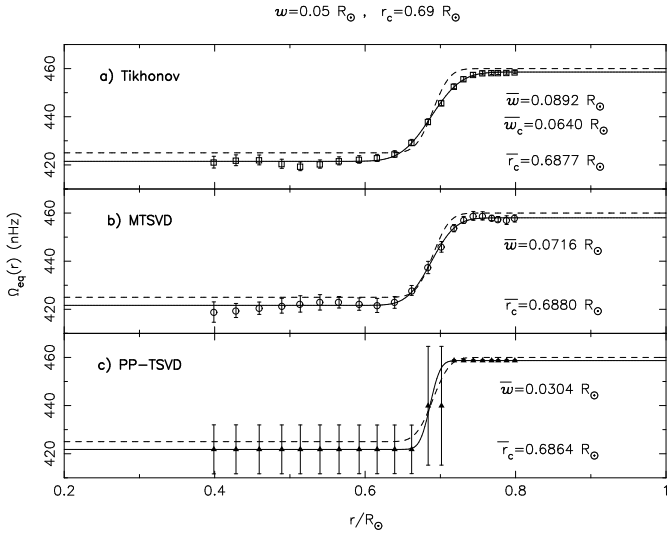

Fig. 5a–c. Solutions obtained between 0.4 and $0.8R_\odot$ from the three inverse methods with the GCV choice of regularization parameters. The input rotation law was the same as in Figs. 2, 4 ('realistic case'). The equatorial component of the initial law is shown by dashed line whereas the fits of the inverse solutions are shown by full lines.

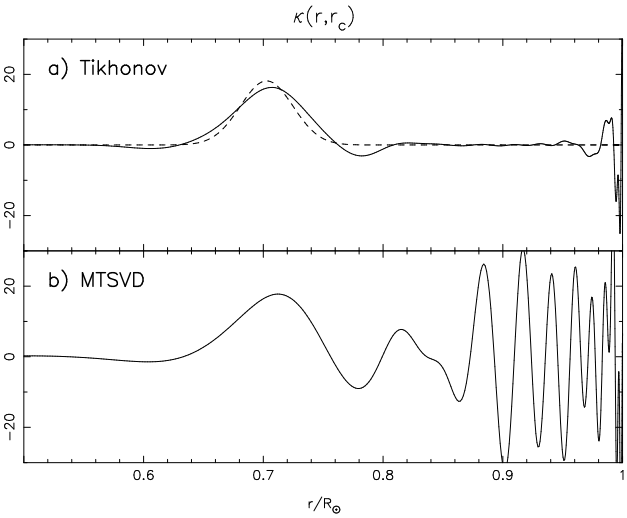

Fig. 6a and b. Averaging kernels computed at $r_0 = \bar{r}_c$. For Tikhonov method the dashed line represents the Gaussian approximation of the kernel used for the local deconvolution of the solution shown on Fig. 5a.

Similar figures (Figs. 3, 4) can be plotted for MTSVD and PP-TSVD methods where the continuous regularization parameter is replaced by the discrete truncation parameter. Results obtained in the 'realistic case' (Fig. 4) have again a larger dispersion and exhibit the same systematic deviation for the determination of Ω_0. Another interesting point is that, as shown on Figs. 3d, 4d and also in the next section, the PP-TSVD method tends to give an under-estimation of the width whereas the MTSVD method tends to give an over-estimation of this parameter. This may be very useful in order to give a bounded estimation of the true width. For these two methods, the choice of the optimal truncation parameter k through the L-curve criterion needs the evaluation of the curvature of discrete L-curve. This can be done carefully by an appropriate 2D curve fitting. Nevertheless our experience shows that it is difficult to do this systematically with the same fit procedure for any level of noise and input rotation law. Furthermore, when this is done carefully, this choice leads to results for the tachocline profile that are always worse than the ones obtained from the GCV choice. Thus, in the following, results are shown only with the GCV criterion for MTSVD and PP-TSVD methods.

Fig. 5 shows the solutions obtained from the three methods with the GCV choices indicated on Figs. 2 and 4. The error bars on the PP-TSVD method (Fig. 5c) were obtained by assuming that the method is linear i.e. the dependence of $\boldsymbol{H}$ (defined in Eq. (A16)) relatively to the data vector $\boldsymbol{W}$ is neglected. This is indeed not the case and a Monte-Carlo approach for estimating errors may be more realistic. We note however that the two other methods (Tikhonov and MTSVD) are linear only for a given regularization parameter. Since this parameter is chosen through automatic strategies, it depends also on the data. Thus, strictly speaking, these methods are also non-linear methods. Nevertheless, the automatic choices are built so that they are not too much sensitive to little change in the data and that justify the linear approximation. The corresponding averaging kernels computed at $r = \bar{r}_c$ (Fig. 6) show that whereas the Gaussian approximation is rather good for the Tikhonov method, the large oscillations in the convection zone obtained for the MTSVD method make difficult the use of a local deconvolution in that case.

4.2. Tests for width between 0.03 *and* 0.11 $R_\odot$

An important point is to test the ability of a method to give a good estimation of the erf-parameters for a large domain of

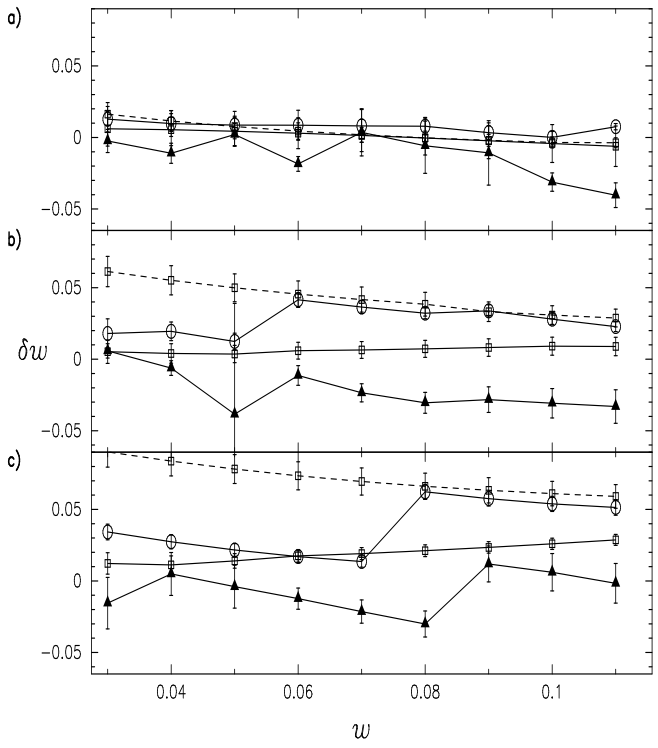

Fig. 7a–c. Difference between the inferred width and the initial width ($\delta w = \bar{w} - w$) against the initial width for PP-TSVD (triangles) and MTSVD (circles) methods, both computed with the GCV choice for the truncation parameter. Squares are for the Tikhonov method with GCV criterion (full line) and L-curve criterion (dashed line). For this latter method we plot the difference between the corrected inferred width and the initial width ($\delta w = \bar{w}_c - w$). **a** $k_\sigma = 10$, $A = B = 0$ as in Figs. 1, 3 ('ideal case'); **b** $k_\sigma = 1$, $A = B = 0$; **c** $k_\sigma = 1$, $A = 55$, $B = 75$ as in Figs. 2, 4 ('realistic case')

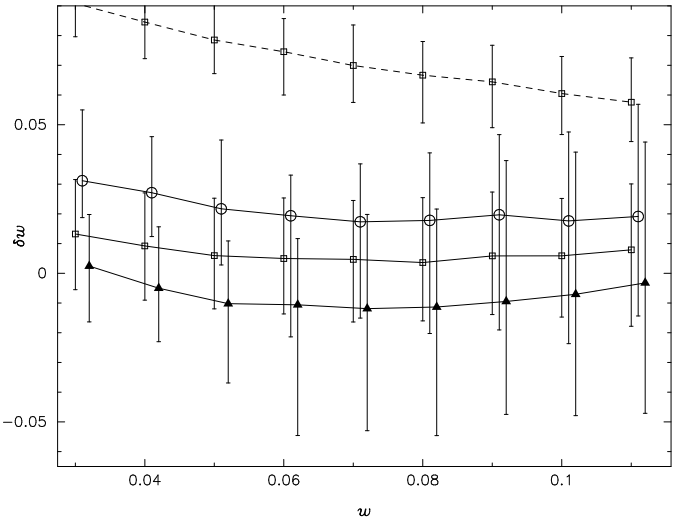

Fig. 8. The same as in Fig. 7c ('realistic case') but each points is the mean value of the results obtained for 500 realizations of input errors. Error bars represent a 68.3% confidence interval on w.

variation of the width of the tachocline. We first study in Fig. 7 the behavior of the different methods and automatic strategies between the 'ideal case' and the 'realistic case' for one realization of input errors. Then, in Fig. 8, we have carried out a Monte-Carlo approach in order to have a better estimation of the errors on the widths deduced from the fit of the solutions for the 'realistic case'.

Fig. 7 shows the inferred width $\bar{w}$ (for MTSVD and PP-TSVD methods) and the corrected inferred width $\bar{w}_c$ (for the Tikhonov method) as functions of the initial width w and for one realization of the input errors. Fig. 7a represents the same example as Figs. 1, 3 ('ideal case'), in Fig. 7b we increase the level of noise ($k_\sigma = 1$), and finally we set an input rotation law with a latitudinal dependence in the convection zone so that the Fig. 7c is for the same example as Figs. 2, 4 ('realistic case').

In Fig. 7a , the results for $\bar{w}$ fit the real value within $0.02R_\odot$ except for PP-TSVD and widths above $0.9R_\odot$, and the two regularization procedures (L-curve and GCV) give almost the same result.

The comparison of Figs. 7a and 7b clearly indicates that the results obtained for Tikhonov method with the L-curve criterion (dashed curves) are very sensitive to the level of noise and are not adapted to the actual errors of observed data. The deconvolution method using Tikhonov inversion with GCV criterion appears to be the less sensitive to the noise level and the most stable for widths between 0.03 and $0.11R_\odot$. We see again that the results obtained from MTSVD and PP-TSVD lead respectively to an over-estimation and an under-estimation of the real width. Fig. 7c illustrates the effect of a latitudinal dependence of the rotation in the convection zone: an increasing over-estimation of w from the Tikhonov method with GCV criterion and a general larger dispersion of the results.

In Fig. 8, we have performed 500 realizations of input errors for each initial width and each point shown in this figure represents the mean value of the 500 inferred or corrected inferred widths for a given initial width and a given method. Error bars represent a 68.3% confidence interval which contains the nearest 341 inferred widths from the mean value but they are not necessarily symmetric around this value. This study shows that the Tikhonov and PP-TSVD methods with the GCV criterion are the most reliable for estimating the width in the most realistic case. They lead, respectively to an over-estimation and under-estimation of the width of about $0.01R_\odot$ at the maximum for initial widths between $0.03R_\odot$ and $0.11R_\odot$. In that range, the standard deviation obtained for 500 realizations of input errors is around $0.02R_\odot$ for Tikhonov method and much larger (up to $0.05R_\odot$ for $w = 0.11R_\odot$) for PP-TSVD method which then appears to be well adapted only to infer very sharp transitions. Let ω_i represent the widths deduced from N_r hypothetical (non-observed) realizations of the unknown true width $\hat{\omega}$. In the Monte-Carlo method we suppose that we can approximate the distribution of $(\hat{\omega} - \omega_i,\ i = 1, ..N_r)$ by the distribution of $(\omega_o - \tilde{\omega}_i,\ i = 1, N_r)$ where ω_o is the width deduced from the observed dataset and $\tilde{\omega}_i$ are the widths deduced from datasets built by setting $\hat{\omega} = \omega_o$ in the model. As we can not insure that ω_o

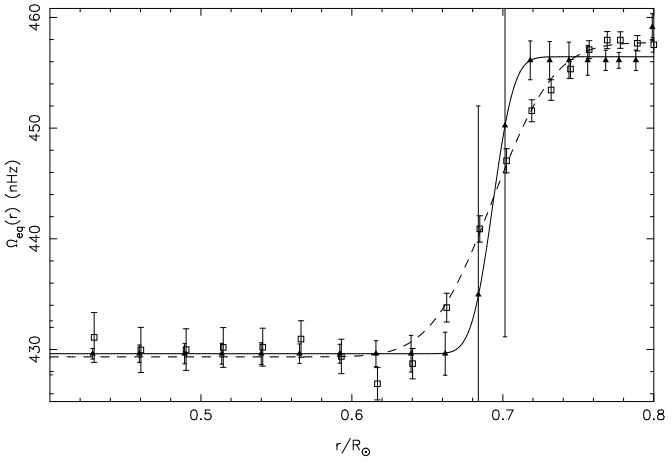

Fig. 9. Equatorial tachocline profiles obtained from LOWL data by PP-TSVD (triangles) and Tikhonov (squares) methods with GCV criterion. Error bars represent the 1σ errors estimated on the solution by assuming the linearity of the inversions. The full and dashed curves represent respectively the fit of the PP-TSVD and Tikhonov solutions by an erf-function between 0.4 and $0.8R_\odot$.

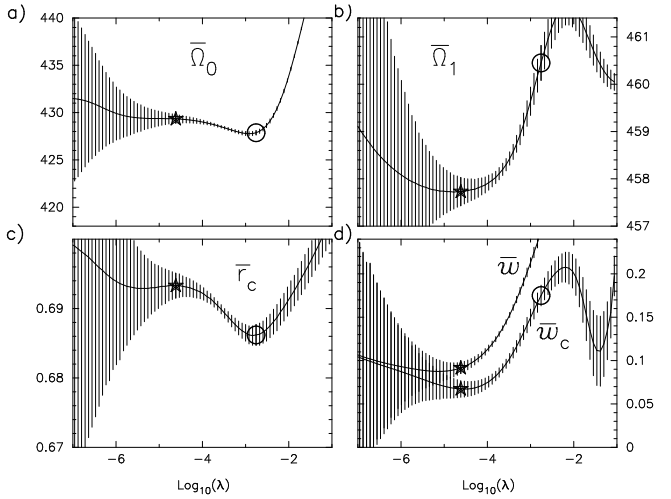

Fig. 10a–d. Variation of the inferred parameters $\bar{\Omega}_0, \bar{\Omega}_1, \bar{r}_c, \bar{w}$ and $\bar{w}_c$ as a function of the logarithm of the regularization parameter for the Tikhonov inversion of LOWL data. Graph markers have the same meaning as in Fig. 1. The L-curve choice of $\bar{w}$ is outside the plot on panel **d**.

is very close to $\hat{\omega}$, the underlying assumption is that, in the range of uncertainty concerning $\hat{\omega}$ (say $0.03 - 0.11R_\odot$), the way in which errors propagate through the inverse process does not vary rapidly (see e.g. Press et al. 1992). The fact that, in Fig. 8, error bars grow rapidly with the initial width for PP-TSVD method makes difficult the use of the Monte-Carlo results for estimating the statistical behavior of this method. There are nevertheless two factors that may introduce bias in these estimations of the errors on the inferred widths. First, the existing correlations between the inferred rotation values obtained at two different radius are not taken into account in the fit of the solution by an erf-function. Secondly, for the PP-TSVD method, the non-linearity of the method is not taken into account in the estimation of the propagation of noise through the inverse process. Making the fit in the right way, i.e. taking into account correlations, may lead to a lower dispersion of the results and then our estimation of the error on the inferred widths may be over-estimated. Nevertheless, the effects of these two approximations are not easy to estimate a priori and need a more complete analysis in future work.

5. Results for LOWL data

This section gives the results obtained from the two years (2/26/94-2/25/96) observations by the LOWL instrument in Hawaii (Tomczyk et al. 1995; Corbard et al. 1997). These data contain 1102 modes with degrees up to l = 99 and frequencies between 1200 and 3500 μHz. For each mode (n, l), individual splittings are given by, at best, five a-coefficients of their expansion on orthogonal polynomials defined by Schou et al. (1994). For this work, we assume that the previous simulations provide an estimation of the bias introduced by the methods and we use these values in order to correct the inferred tachocline parameters. This supposes the closeness of the model used in the simulation to the reality and a good estimation of the errors in the data. Furthermore, we use the sum of odd a-coefficients as a first approximation for the sectoral splittings i.e. $\Delta\nu_{nll} \simeq a_1^{nl} + a_3^{nl} + a_5^{nl}$. This approximation is exact for all the rotation laws such that $a_{2j+1}^{nl} = 0 \; \forall \; j > 2$ (which is the case for the rotation laws Eq. 4 used in our model). When this is not the case the latitudinal kernel associated to $a_1^{nl} + a_3^{nl} + a_5^{nl}$ is less peaked at the equator than the one associated to the sectoral splittings (i.e. $P_l^l(\cos\theta)^2 \sin\theta$, see Sect. 2) and thus $\hat{\Omega}_1$ represents a latitudinal average of the rotation in a larger domain around the equator. However the kernel associated to the sum of three a-coefficients is less l-dependent.

Results obtained by the three methods are summarized in Table 1. They are in very good agreement for the location of the tachocline and the mean values of the rotation rate in the radiative interior and convection zone but more dispersive concerning the determination of the width. The tests discussed above have shown that this may be related to the level of noise contained in the data. The equatorial tachocline profiles obtained by Tikhonov and PP-TSVD methods with GCV criterion are shown in Fig. 9. According to the previous sections, we use the GCV choice in order to infer the location and the width of the equatorial tachocline. Nevertheless, for Ω_0 and Ω_1 the L-curve choices may be useful in order to see the amplitude of the variation of the inferred parameters against the regularization parameter. The errors cited in this table are just the result of the fit of the solution by the erf-function. The variation of the inferred erf parameters against the regularization, as shown by Fig. 10 for the Tikhonov method, and the previous Monte-Carlo simulations can help us to estimate error bars that may be more realistic.

Table 1. Inferred erf-parameters obtained from LOWL data. The L-curve criterion has not been used for methods with discrete truncation parameters.

Methods	$\bar{\Omega}_0$ (nHz)		$\bar{\Omega}_1$ (nHz)		$\bar{r}_c/R_\odot$	$\bar{w}_{(c)}/R_\odot$
	GCV	L-curve	GCV	L-curve	GCV	GCV
Tikhonov	429.3 ± 0.5	427.9 ± 0.3	457.7 ± 0.3	460.4 ± 0.4	0.693 ± 0.002	0.067 ± 0.010
MTSVD	429.4 ± 0.7	-	457.0 ± 0.5	-	0.693 ± 0.003	0.062 ± 0.009
PP-TSVD	429.6 ± 0.2	-	456.4 ± 0.3	-	0.693 ± 0.009	0.031 ± 0.017

Fig. 10a shows that the evaluation of the mean value of the rotation rate in the radiative interior ($\hat{\Omega}_0$) is not much sensitive to the regularization. Nevertheless, we have shown in Sect. 4.1 that this parameter tends to be systematically under-estimated of about 4 nHz because of the influence of the latitudinal variation of the rotation in the convection zone on the low l sectoral splittings. For the sum a_1^{nl} + a_3^{nl} + a_5^{nl} the latitudinal kernel is less l-dependent so that this systematic offset may be smaller than 4 nHz. We take this effect into account by increasing the estimation of the error and our final interval for this parameter becomes: $427.5 \leq \hat{\Omega}_0 \leq 434.5$ nHz. The mean value of the equatorial rotation rate in the convection zone is less subject to systematic errors but may be under-estimated by the GCV choice (cf. Figs. 2b, 4b, 5). The difference between the GCV choice and the L-curve choice is about 3 nHz on Fig. 10. Thus we estimate that $\hat{\Omega}_1 = 459.0 \pm 1.5$ nHz. We note that we do not attempt to use the points of the solution found under $0.4R_\odot$ or above $0.8R_\odot$ (cf. Fig. 9). Therefore $\hat{\Omega}_1$ does not take into account the eventual rapid variation of the rotation near the surface or at $0.9R_\odot$ (Antia et al. 1996) and $\hat{\Omega}_0$ is not sensitive to the core rotation. The ratio $q = \hat{\Omega}_0/\hat{\Omega}_1$ obtained from helioseismic data is an important test for the theories of the tachocline dynamics. Spiegel and Zahn's (1992) theory leads to $q = 0.90$ whereas Gough's (1985) one leads to $q = 0.96$. Our results give $0.93 < q < 0.95$ which is intermediate between the two theoretical estimates. Similar results have already been pointed out by Gough & Sekii (1997).

For the estimation of $\hat{r}_c$, we find in Fig. 10 that the L-curve criterion leads to a lower value than the GCV criterion as we had found in Fig. 2. As discussed in Sect. 4.1, we think that the GCV choice is more reliable but may lead to an under-estimation of about $0.002R_\odot$. Therefore our final estimation for the location of the center of the tachocline in the equatorial plane is: $\hat{r}_c = 0.695 \pm 0.005R_\odot$. This value, estimated in the equatorial plane, is intermediate between the two values previously obtained by forward methods (cf. Table 2). We note however that whereas our work just look for the equatorial component of the tachocline, the previous works assume that the solar tachocline presents the same profile at any latitude. This may lead to bias if, as suggested by Charbonneau et al. (1997) from LOWL data, the tachocline is prolate i.e. is located deeper at the equator than at higher latitudes.

The tests discussed in the previous sections show that the L-curve choice is not reliable for the estimation of the width and suggest three ways for estimating the width of the tachocline from GCV criterion:

First, the true value is supposed to lie between the MTSVD and PP-TSVD estimations. That gives $0.031R_\odot \leq \hat{w} \leq 0.062R_\odot$.

Secondly, for the Tikhonov method, since the error bars have roughly of the same amplitude in the whole range $0.03-0.11R_\odot$ of initial widths (Fig. 8) , we can use the Monte-Carlo simulation. Near $w = 0.07R_\odot$ (the inferred value reported in Table 1 being $\bar{w} = 0.067$), Fig. 8 shows that the Tikhonov method leads in mean to a systematic over-estimation of about $0.005R_\odot$ with a 68.3% confidence interval around $\pm 0.02R_\odot$. Thus we obtain by this way $\hat{w} \simeq 0.062 \pm 0.020R_\odot$.

Thirdly, the PP-TSVD method is though to produce, in mean, an under-estimation of the width of about $0.01R_\odot$ but with a larger dispersion of the results for the large widths so that we are not allowed to use straightforwardly our Monte-Carlo simulation. The 68.3% confidence intervals plotted in Fig. 8 indicate that the PP-TSVD method can lead to an inferred width around $0.03R_\odot$ (which is the value obtained from LOWL data) for initial widths up to $0.08R_\odot$. Therefore the interpretation of the result obtained by this method is not easy. This may indicate that the method is better suited to the search of transition zones known a priori to be very thin (searching for a width lower than $0.05R_\odot$ for example). Nevertheless, all the above discussions indicate $0.020 \leq \hat{w} \leq 0.070R_\odot$ as a reasonable interval for the true width, deduced from PP-TSVD method.

All these approaches are globally consistent but lead to a relatively large dispersion of the results. Therefore our final estimation of the width of the solar tachocline in the equatorial plane is: $\hat{w} = 0.05 \pm 0.03R_\odot$. This estimation is in very good agreement with the result obtained by Charbonneau et al. (1997) and remains compatible with the value given by Kosovichev (1996) (cf. Table 2).

6. Conclusions

This work presents an analysis of the determination of the characteristics of the tachocline at the equator by three different inverse methods. They are applied to the inversion of the splittings of the sectoral modes estimated as the sum of the three first odd coefficients of the expansion of the splittings in orthogonal polynomials defined by Schou et al. (1994). Two different choices of regularization parameters, the GCV and L-curve criteria, have

Table 2. Comparison of our results with previous forward analysis. Charbonneau et al. (1997) and our work are for the same LOWL dataset (2/26/94-2/25/96) whereas Kosovichev (1996) has used the 1986-90 BBSO datasets.

	$\hat{r_c}/R_\odot$	$\hat{w}/R_\odot$
This work	0.695 ± 0.005	0.05 ± 0.03
Charbonneau et al.	0.704 ± 0.003	0.050 ± 0.012
Kosovichev	0.692 ± 0.005	0.09 ± 0.04

been compared. Tests with artificial rotation laws have shown that in all cases the GCV criterion is less sensitive to the error level than the L-curve one and gives better results with low bias and dispersions in the range $0.03 - 0.011 R_\odot$ of searched widths. This choice of the GCV criterion is in agreement with Barett (1993) and Thompson(1992) in another context. Hansen (1992) has shown that the GCV criterion is less adapted to highly correlated errors than the L-curve one. Our work may indicate in turn that we can neglect, as it has been done, the unknown correlation in LOWL data.

Concerning the thickness of the tachocline, it appears that the MTSVD and PP-TSVD inversions give respectively an upper and lower estimate while the Tikhonov method corrected by deconvolution gives the most reliable determination. We have estimated the systematic effect of the latitudinal dependence of the rotation in the convection zone on the determination of the thickness of the tachocline and the rotation in the radiative interior. We have shown how the performance of the methods will be improved by lowering the level of noise in the data.

The methods have been applied to the LOWL two years dataset leading to an estimation of the position $\hat{r}_c = 0.695 \pm 0.005 R_\odot$ and the thickness $\hat{w} = 0.05 \pm 0.03 R_\odot$ of the equatorial tachocline. In addition, we have obtained an estimation of the equatorial rotation $\hat{\Omega}_0$ below the convection zone and above $0.4 R_\odot$ such that: $427.5 \leq \hat{\Omega}_0 \leq 434.5$ nHz and $\hat{\Omega}_1$ from the top of the convection zone up to $0.8 R_\odot$ such that $\hat{\Omega}_1 = 459.0 \pm 1.5$ nHz. Assuming that the rotation in the radiative interior is independent of latitude, this leads to a ratio $\hat{\Omega}_0/\hat{\Omega}_1$ between 0.93 and 0.95 which is intermediate between the two theoretical predictions.

Our results for the location and thickness of the equatorial tachocline are in agreement with the forward analysis of Charbonneau et al. (1997) and with those of Basu applied on BBSO and GONG datasets (Basu 1997) using a different parameterization of the tachocline. The forward analysis can be viewed as non-linear least-squares methods (least-squares methods because of the use of the χ^2 criterion and non linear because of the models used for the rotation profile) but using only a very few number of parameters (Charbonneau et al. (1997) use six parameters, Basu (1997) three and Kosovichev (1996) only two). This kind of methods depend thus strongly on our knowledge of the global rotation profile which can be reached only by inversion techniques. In particular, in the above-cited works the latitudinal dependence of the rotation is fixed (as in 1.5D inversions). In this work, we have tried to investigate the amount of informations about the tachocline that we can extract directly from the global inversions without a-priori knowledge (except for the regularization) on the rotation profile. There are less assumptions in this approach, and thus the tachocline parameters may be less constrained. The fact that the two approaches lead to similar results indicates in turn that the hypothesis used in the forward analysis are probably not too strong and are well adapted to the problem of inferring the tachocline from actual data.

One of the interest of this work was our first attempt to use an inverse method with non-linear regularization in helioseismic case. The PP-TSVD method leads to a very large dispersion of the results for widths above $0.05 R_\odot$ and then is difficult to interpret with actual data. Some efforts, in future work, should be useful to improve this kind of methods and the interpretation of their results taking into account their non-linearity.

Acknowledgements. We gratefully acknowledge T. Sekii for illuminating discussions and comments, S. Tomczyk and J. Schou for providing the LOWL data and the anonymous referee for constructive comments.

Appendix A: details of the three inverse methods used

We discretize Eq. (2) by:

$$\boldsymbol{W} = \boldsymbol{R\Omega} \tag{A1}$$

where we have defined:

$$\boldsymbol{W} \equiv (W_i)_{i=1,N} \qquad W_i = \Delta\nu_{nll} + \delta\nu_{nll},\ i \equiv (n,l), \tag{A2}$$

N being the number of modes (n,l) ($N = 1102$ for LOWL data) and $\delta\nu_{nll}$ a normally distributed noise with a standard deviation defined in Eq. (5). We search the solution $\bar{\Omega}(r)$ as a piecewise linear function of the radius by setting:

$$\bar{\Omega}(r) = \sum_{p=1}^{N_p} \omega_p \varphi_p(r) \qquad \boldsymbol{\Omega} \equiv (\omega_p)_{p=1,N_p} \tag{A3}$$

where $\varphi_p(r)$, $p = 1, N_p$ are piecewise straight lines ($N_p = 50$ in this work) such that:

$$\forall p = 1..N_p,\ \exists\, r_p \in [0.,1.] \,/\, \bar{\Omega}(r_p) = \omega_p \tag{A4}$$

where r_p, $p = 1..N_p$ are fixed break points distributed according to the density of turning points of modes (Corbard et al., 1997). The matrix $\boldsymbol{R}$ is then defined by:

$$\boldsymbol{R} \equiv (R_{ip})_{\substack{i=1,N \\ p=1,N_p}} \qquad R_{ip} = \int K_{nl}(r)\varphi_p(r)dr \tag{A5}$$

For all the inverse methods discussed in this work, the aim is to find a solution that is able to produce a good fit of the data in chi-square sense. Unfortunately, the solution of this problem is not unique and allows oscillatory solutions that are not physically acceptable. So, we have to define a quantity that measures the smoothness of the solution and to insure that the final solution is sufficiently smooth to be acceptable.

For any solution $\mathbf{\Omega}$, we define the χ^2 value by:

$$\chi^2(\mathbf{\Omega}) = \|\boldsymbol{P}(\boldsymbol{R}\mathbf{\Omega} - \boldsymbol{W})\|_2^2 \tag{A6}$$

where $\boldsymbol{P} = diag(1/\sigma_{nl})$ and we define two measures of the smoothness of the solution $\mathbf{\Omega}$ by:

$$\beta_i(\mathbf{\Omega}) = \|\boldsymbol{L}\mathbf{\Omega}\|_i,\ i = 1, 2 \tag{A7}$$

where the vector i-norms $\|.\|_i$ are defined by $\|\boldsymbol{x}\|_i = (\sum_p |x_p|^i)^{1/i}$ and $\boldsymbol{L}$ is a discrete approximation of the first derivative operator such that:

$$\beta_1 \propto \int \left|\frac{\partial\Omega(r)}{\partial r}\right| dr \qquad \beta_2^2 \propto \int \left(\frac{\partial\Omega(r)}{\partial r}\right)^2 dr \tag{A8}$$

A.1. Tikhonov solution

The so called Tikhonov solution $\mathbf{\Omega}_\lambda$ solves the problem:

$$\min_{\mathbf{\Omega}} (\chi^2(\mathbf{\Omega}) + \lambda\beta_2^2(\mathbf{\Omega})), \tag{A9}$$

where $\lambda > 0$ is the continuous regularization parameter. In order to compare this method to the two other ones, it may be interesting to reformulate the problem as follow: For any λ we can show that there exist a value $\alpha(\lambda)$ for which $\mathbf{\Omega}_\lambda$ is the solution of the problem:

$$\min_{\mathbf{\Omega}\in S_\lambda} \beta_2(\mathbf{\Omega}); \quad S_\lambda = \{\mathbf{\Omega} \,/\, \|\boldsymbol{P}(\boldsymbol{R}\mathbf{\Omega} - \boldsymbol{W})\|_2 \leq \alpha(\lambda)\} \tag{A10}$$

The computation of these solutions for different regularization parameters have been carried out by using a generalized singular value decomposition of the pair $(\boldsymbol{R}, \boldsymbol{L})$ as explained and discussed extensively in Christensen-Dalsgaard et al. (1993).

A.2. MTSVD and PP-TSVD solutions

These methods are based on the SVD of the $N \times N_p$ $(N > N_p)$ matrix $\boldsymbol{R}$ which can be written:

$$\boldsymbol{R} = \sum_{i=1}^{r} \boldsymbol{u}_i \Lambda_i \boldsymbol{v}_i^\top \tag{A11}$$

where $r \leq N_p$ is the rank of $\boldsymbol{R}$. The singular vectors are orthonormal, $\boldsymbol{u}_i^\top \boldsymbol{u}_j = \boldsymbol{v}_i^\top \boldsymbol{v}_j = \delta_{ij}$ for $i, j = 1, r$, and the singular values Λ_i are such that: $\Lambda_1 \geq \Lambda_2 \geq ... \geq \Lambda_r > 0$, $\Lambda_{r+1}, .., \Lambda_{N_p} = 0$. We then define the the TSVD of $\boldsymbol{R}$ as the matrix $\boldsymbol{R}_k$ built from Eq. (A11) but neglecting the $N_p - k$ smallest singular values.

$$\boldsymbol{R}_k = \sum_{i=1}^{k} \boldsymbol{u}_i \Lambda_i \boldsymbol{v}_i^\top \tag{A12}$$

The integer $k < r$ is called the truncation parameter. It acts as a regularization parameter by eliminating the oscillatory behavior of the singular vectors associated with the smallest singular values. According to Eq. (A12), the rank of the matrix $\boldsymbol{R}_k$ is $k < r$ and then the problem of minimizing the quantity $\|\boldsymbol{P}(\boldsymbol{R}_k\mathbf{\Omega} - \boldsymbol{W})\|_2$ has not an unique solution and we have to use our smoothness criteria to select a physically acceptable solution among the set of solutions defined by:

$$S_k = \{\mathbf{\Omega} \,/\, \|\boldsymbol{P}(\boldsymbol{R}_k\mathbf{\Omega} - \boldsymbol{W})\|_2 = \text{minimum}\} \tag{A13}$$

With these notations, the so-called MTSVD solution $\mathbf{\Omega}_k^m$ is defined by:

$$\mathbf{\Omega}_k^m = \arg \min_{\mathbf{\Omega}\in S_k} \beta_2(\mathbf{\Omega}) \tag{A14}$$

whereas the so-called PP-TSVD solution $\mathbf{\Omega}_k^p$ is defined by:

$$\mathbf{\Omega}_k^p = \arg \min_{\mathbf{\Omega}\in S_k} \beta_1(\mathbf{\Omega}) \tag{A15}$$

The algorithms for computing these solutions are presented in Hansen et al. (1992) and Hansen & Mosegaard (1996) respectively.

We just recall some important properties of the PP-TSVD solution: For any $k < r$ the vector $\boldsymbol{L}\mathbf{\Omega}_k^p$ has at the most $k - 1$ non zero elements. As the matrix $\boldsymbol{L}$ is a discrete approximation of the first derivative, this means that the solution vector $\mathbf{\Omega}_k^p$ consists on $k_b \leq k$ constant blocks. From Eq. (A3) it follows that the inferred rotation $\widetilde{\Omega}(r)$ itself is obtained as a piecewise constant functions with a maximum of k pieces. The $k_b - 1$ break points of this solution are selected by the procedure among the N_p initials break points r_p. Therefore this inversion is able to produce a discontinuous solution without fixing a-priori the location of the discontinuity. Finally, we note that the solution $\mathbf{\Omega}_k^p$ obtained by this non-linear method can always be computed by applying a matrix $\boldsymbol{H}$, to the data but this matrix is also a function of the data i.e. $\boldsymbol{H} = \boldsymbol{H}(\boldsymbol{W})$. Thus we have:

$$\mathbf{\Omega}_k^p = \boldsymbol{H}(\boldsymbol{W})\boldsymbol{W}. \tag{A16}$$

References

Antia H.M., Chitre S.M., Thompson M.J., 1996, A&A 308, 656

Aubert G., Barlaud M., Blanc-Féraud L., Charbonnier P., 1994, Deterministic edge-preserving regularization in computed imaging, Reasearch Report no. 94-01, Univ. of Nice-Sophia Antipolis

Badeva V., Morozov V., 1991, Problèmes incorrectement posés - Théorie et applications, série Automatique, Mason, Paris

Barrett R.K., 1993, On the optimal choice of regularization parameter for the inversion of solar oscillation data. In: Brown T.M. (ed) GONG 1992: Seismic Investigation of the Sun and Stars (A.S.P. Conf. Ser. vol. 42), Astr. Soc. of the Pacific, San Francisco, p. 233

Basu S., 1997, MNRAS 288, 572

Charbonneau P., Christensen-Dalsgaard J., Henning R., et al., 1997, Observational constraints on the dynamical properties of the shear layer at the base of the solar convection zone. In: Provost J., Schmider F.X. (eds) Sounding solar and stellar interior, poster volume, OCA, in press

Christensen-Dalsgaard J., Hansen P.C., Thompson M.J., 1993, MNRAS 264, 541

Corbard T., Berthomieu G., Morel P., et al., 1997, A&A 324, 298

Golub H., Heath M., Wahba G., 1979, Technometrics 21, 215

Gough D.O., 1985, In: Future mission in solar heliosphere and space plasma physics, eds. E. Rolfe and B. Battrick, ESA publication division, SP-235, p.183
Gough D.O., Sekii T., 1997, On the solar tachocline. In: Provost J., Schmider F.X. (eds) Sounding solar and stellar interior, poster volume, OCA, in press
Hansen P.C., 1992, SIAM Review 34, 561
Hansen P.C., 1994, Numerical Algorithms 6, 1
Hansen P.C., Mosegaard K., 1996, Piecewise Polynomials Solutions Without a Priori Break Points, Numerical Linear Algebra with Applications 3 (6), 513
Hansen P.C., Sekii T., Sibahashi H., 1992, SIAM J. Sci. Stat. Comput. 13, 1142
Kosovichev A.G., 1996, ApJ 469, L61
Morel P., Provost J., Berthomieu G., 1997, A&A 327, 349
Pijpers F.P., Thompson M.J., 1992, A&A 262, L33
Pijpers F.P., Thompson M.J., 1994, A&A 281, 231
Press W.H., Teukolsky S.A., Vetterling W.T., Flannery B.P., 1992, Numerical Recipes (2nd Edition), Cambridge Univ. Press
Schou J., Christensen-Dalsgaard J., Thompson M.J., 1994, ApJ 433, 389
Sekii T., Shibahashi H., 1988, An inversion method based on the Moore-Penrose generalized inverse matrix. In: Seismology of the Sun and Sun-Like Stars, Rolfe E.J. (ed) ESA SP-286, ESA Publication Division, Noordwijk, the Netherlands, p. 521
Snodgrass H.B., Ulrich R.K., 1990, ApJ 351, 309
Spiegel E.A., Zahn J.-P., 1992, A&A 265, 106
Stepanov A.A., Christensen-Dalsgaard J., 1996, On the choice of tradeoff parameter in helioseismic SOLA inversion. In: B.H. Jacobsen, K. Mosegaard & P. Sibani (eds) Proc. Interdisciplinary Inversion Conference, University of Aarhus, May 22-24 1995, Lecture Notes in Earth Sciences 63, Springer, p. 54
Thompson A.M., 1992, A&A 265, 289
Thompson A.M., Craig I.J.D., 1992, A&A 262, 359
Thompson M.J., Toomre J., et al., 1996, Science 272, 1300
Tikhonov A.N., Arsenin V.Y., 1977, Solutions of Ill-Posed Problems, Winston, Washington D.C.
Tomczyk S., Streander K., Card G., et al., 1995, Solar Phys. 159, 1
Vogel C.R., Oman M.E., 1996, SIAM Journal of Scientific Computing, vol. 17, No. 1
Vogel C.R., Oman M.E., 1997, IEEE Transactions on Image Processing, submitted
Wahba G., 1977, SIAM J. Numer. Anal. 14, 651

This article was processed by the author using Springer-Verlag LaTeX A&A style file *L-AA* version 3.